Mechanics of Materials 132 (2019) 57–65

Contents lists available at ScienceDirect

Mechanics of Materials

journal homepage: www.elsevier.com/locate/mechmat

Research paper

Mechanical reinforcement of methylcellulose hydrogels by rigid particle additives

Yonatan Rotbaum[a,*,1], Galit Parvari[b,1], Yoav Eichen[b], Daniel Rittel[a]

[a] Faculty of Mechanical Engineering, Technion, Haifa 3200008, Israel
[b] Schulich Faculty of Chemistry, Technion, Haifa 3200008, Israel

ARTICLE INFO

Keywords:
Methyl cellulose hydrogels
Thermoreversible gelation
Mechanical properties
Static compression
Dynamic compression
Nano-particles

ABSTRACT

Methylcellulose hydrogels are attracting considerable interest due to their unique thermo-reversible gelation. The present work focuses on the attempt to tune, control and improve the mechanical response of these hydrogels by using silica (SiO_2), alumina (Al_2O_3) and boron carbide (B_4C) particles, while preserving their ability to thermo-gelate. A systematic experimental study reveals the dependence of the flow stress of the hydrogel-composite on the type and size of particle additive. Methylcellulose composite hydrogels also show increased flow-stress dependence on temperature, compared to the parent hydrogel. Similarly, some of these novel composite exhibit very high strain-rate sensitivity, with up to 90 times increase of strength in the dynamic regime. Thus, the present study offers simple tools to fine-tune the mechanical properties of these highly applicable methylcellulose hydrogels, by using small amounts of additives. Of the studied composites, the best results for dynamic flow-stress increase were achieved with nanometric boron carbide particles. This could be due to the large surface area for interaction with the methylcellulose and with the particles serving as heterogenic focal points for phase-transition.

1. Introduction

The ability to produce hydrogels with controlled properties has motivated generic and industrial-oriented research and developments over the last decades. Hydrogels are used in a variety of fields for a wide range of applications, ranging from simple suspensors for shock absorbers, acoustic insulators and bulkhead seals (Serra, 2002; Borzacchiello and Ambrosio, 2009), to drug delivery agents (Chang and Zhang, 2011; Wang et al., 2009), tissue engineering (Hu et al., 2010; Yahia et al., 2015), tissue mimicry and stimuli sensors (Richter et al., 2008; Peppas et al., 2010; Gaharwar et al., 2014).

Aqueous solutions of methylcellulose (MC), a biocompatible synthetically methylated polysaccharide, display an unusual trait: they undergo reversible thermogelation (Sarkar, 1979; Arvidson et al., 2012; Hirrien et al., 1998). This behavior places them in the currently limited family of known inverse-freezing materials – materials which solidify upon heating and liquefy upon cooling (Schupper and Shnerb, 2005). This fascinating phenomenon has been explored by several groups over the past decades, who have gained valuable insights into its mechanisms and affecting factors (Arvidson et al., 2012; Hirrien et al., 1998; Huang et al., 2014; Xu et al., 2004; Lott et al., 2013; Nasatto et al., 2015; Li, 2002; Kobayashi et al., 1999). Solutions of MC and hydrogels of MC (MCH) have found their way into a large variety of applications, among which are in the fields of food and agriculture, cosmetics, pharmaceuticals and even construction (Wang et al., 2009; Nasatto et al., 2015; Plank, 2005). Studies on the mechanical response of MCHs found that even beyond their gelation temperature, their flow-stress increases with temperature (Rotbaum et al., 2017; McAllister et al., 2015). This stands in contrast with the majority of currently known hydrogels and polymeric materials, which soften upon heating. Moreover, while temperature-induced gelation normally takes a upwards of a minute (Hirrien et al., 1998), it has been recently shown that upon impact, MC solutions can transform into a gel state within a few tenths of microseconds (Parvari et al., 2018). This rapid gelation enables these liquids be excellent energy absorbers, since the gelation is endothermic and thus uptakes the energy delivered into the solution by the impact.

With the increasing use of hydrogel-based products, there is an extensive attempt to improve and enhance some of their properties by means of using micro- and nano-sized particle additives (Gaharwar et al., 2014; Haraguchi, 2007; Schexnailder and Schmidt, 2009; Thoniyot et al., 2015; Schmidt and Malwitz, 2003; Kokabi et al., 2007). With proper design considerations, such as the particle properties, uniform and stable dispersion of the particles in the gel, and carefully adjusted particle concentrations, a composite hydrogel can be prepared,

* Corresponding author.
E-mail address: y.rotbaum@gmail.com (Y. Rotbaum).
[1] equal contribution

https://doi.org/10.1016/j.mechmat.2019.02.013
Received 29 November 2018; Received in revised form 7 February 2019
Available online 22 February 2019

which shows improved properties over those of the pristine hydrogel (Gaharwar et al., 2014; Schexnailder and Schmidt, 2009; Thoniyot et al., 2015; Schmidt and Malwitz, 2003; Coleman et al., 2006). For example, silica particles are used to control the opacity of hydrogels, as well as modify the tortuosity and the adhesion forces of certain hydrogels (Elias et al., 2007; Zhang and Archer, 2002). Carbon nanotubes, which are a very common component in a variety of composite engineering materials, can be used to confer (improved) electrical conductivity and provide high longitudinal strength to soft matrices (Shin et al., 2013; Yan et al., 2011; Xie et al., 2010; Zhang et al., 2011). Alumina particles can be used in metals and polymer bulks to increase wear resistance through surface hardness, or to strengthen polymeric matrices (Bhimaraj et al., 2005; Guo et al., 2006).

This work focuses on improving the mechanical properties of methylcellulose-based hydrogels. Specifically, on the attempt to improve the flow-stress of these unique gels by compositing them with micro and nano-sized particles. Controlling and improving the mechanical properties of MCHs is expected to improve their performance as shock mitigators and acoustic insulators, as well as tissue mimickers.

In the first part of the report, the quasi-static mechanical response of particle-MCH composites is characterized for several types of particles (alumina, silica and boron carbide), with emphasis on the particles' type and size.

The second part explores the compressive strain-rate sensitivity of MCH composites in the range of 10^{-3}–10^{3} s^{-1}. The properties of the new composite MCHs are compared to the pristine MCHs tested under similar conditions (Rotbaum et al., 2017).

2. Experimental

2.1. Materials

Methylcellulose powder (SGA7C FG, DOW Chemical Company) was used without further purification. Water was purified by a water purifier (Millipore Milli-Q instrument), having a resistance of 18MΩ.

2.2. Particle additives

All the particles appearing in this work were used as-is, without further purification unless specifically noted: 1. Large micrometric silica powder ("silica gel 60″, 63–200 μm, Merck). 2. Fumed silica nanoparticles (Aerosil 200, Evonik). 3. Micrometric alumina powder (< 10 μm average particle size, Aldrich). 4. Alumina nanowires, (diam. 2–6 nm, length 200–400 nm, Aldrich). 5. Nano-boron carbide powder (45–55 nm hexagonal plates, US Research Nanomaterials, Inc.). 6. Micron-sized boron carbide powder, of wide size distribution (rhombohedral, Inframat Advanced Materials).

For this latter, optical microscopy (Nikon eclipse LV100) reveals that particles ranged in size from a few tenths of μm to several μm, with an average size of ~0.7 μm. SEM (Vega II, Tescan) measurements show that some of the large particles are aggregates of the smaller particles. This powder was used as a source for the two more narrow size distribution powders.

Narrow size distribution boron carbide powder: 50 g of the commercial micron-sized boron carbide powder were added to 100 mL water, mixed, sonicated for 5 min, and then left to sediment for 48 h. The grey opaque liquid was then decanted and centrifuged at 3000 rpm for 15 min. The resulting sediment and supernatant were separated and each was air-dried for about five days, until no mass change was detected on daily weighing. Optical microscopy examination of samples of both portions indicates that their average diameters are about 1–3 μm and 0.5–2 μm respectively.

Pristine and composite gels: 5 mL water were heated to 70 °C in a screw cap vial containing a magnetic stirring bar, then 0.28 g MC powder was added while manually stirring. The homogenously opaque solution was then capped and kept at 70 °C for at least five more minutes. The stirrer was then removed from solution and the capped vial was placed in an ice-bath for one hour, followed by at least overnight at 4–8 °C. Composite gels were prepared in the same manner, but the particle powder was added to the water and sonicated in an ultrasonic bath (AC-120H, MRC) before the water was heated.

2.3. Static compression measurements

Specimens were cast into sealed glass vials with an internal diameter of 18 mm. They were then heated using a hot water bath to 80° ± 2 °C for 4.5 min, until the specimen reached the gel state (non-equilibrated, this time period includes both heating and annealing). Immediately after the heating stage, the gel specimen was carefully extracted out of the vial and sliced into a cylindrical sample with nominal diameter and height of D_0 = 18 mm, L_0 = 10 mm respectively. The whole procedure took approximately 20–40 s, in order to minimize cooling.

Uniaxial quasi-static compression experiments were conducted on a screw-driven testing machine (Instron 4483), equipped with a 500 N load cell and operated under displacement control, with a prescribed crosshead velocity of 3.6 mm/min, corresponding to nominal strain rate of $0.5{\cdot}10^{-3}\,s^{-1}$. The composite MCHs were tested inside a temperature-controlled chamber, at a temperature of 80° ± 3 °C. During the experiments the force (F) and the displacement (ΔL) were recorded at 8 Hz frequency. Since it was noticed that even at strains of 0.8–0.9 no failure of the specimens occurs, the experiments were deliberately terminated at strains in the range of 0.5–0.9.

In order to minimize frictional effects and to avoid barreling of the sample, two custom glass plate adapters were installed on the conventional compression jigs (Miquelard-Garnier et al., 2008). Before each test, the glass plates were wetted with a few drops of water to reduce friction with the gels.

The measured load-displacement curves were reduced into engineering stress-strain curves, where the engineering stress (σ_{eng}) was calculated as the applied load divided by the original cross section area (A_0).

$$\sigma_{eng} = \frac{F}{A_0} \tag{4}$$

Hence, the engineering strain (ε_{eng}) was calculated as

$$\varepsilon_{eng} = \frac{\Delta L}{L_0} \tag{5}$$

Where L_0 is the original specimen gauge-length and ΔL is the measured displacement.

The repeatability and homogeneity of the mechanical properties of the composite MCHs was tested according to previously described procedures. (See Figures S1 and S2 in the Supplementary Material section) (Rotbaum et al., 2017). Since the stress strain curves of the different composite MCHs were found to be very similar, the curves presented in the results section are representative.

2.4. Dynamic compression experiments

Dynamic compression experiments were performed using a conventional 12.7 mm diameter Split Hopkinson pressure bar (SHPB, Kolsky apparatus) (Kolsky, 1949), made of 7075-T6 aluminum-alloy bars, loaded at the far end of the incident bar with a projectile made of the same material. In conventional SHPB setups, the forces and the displacement measurements are usually performed using strain gauges attached to the Hopkinson bars. The strain gauges record the incident, reflected and transmitted stress waves, ε_{inc}, ε_{ref} and ε_{tra} respectively, which are then converted into stress and strain pulses using 1D wave analysis (Lifshitz and Leber, 1994). A representative picture of the modified Kolsky apparatus is shown in Fig. 1.

Examination of soft materials with mechanical impedance significantly lower than that of Hopkinson bars, poses an experimental challenge (Chen et al., 2000; Chen and Song, 2011; Song and Chen,

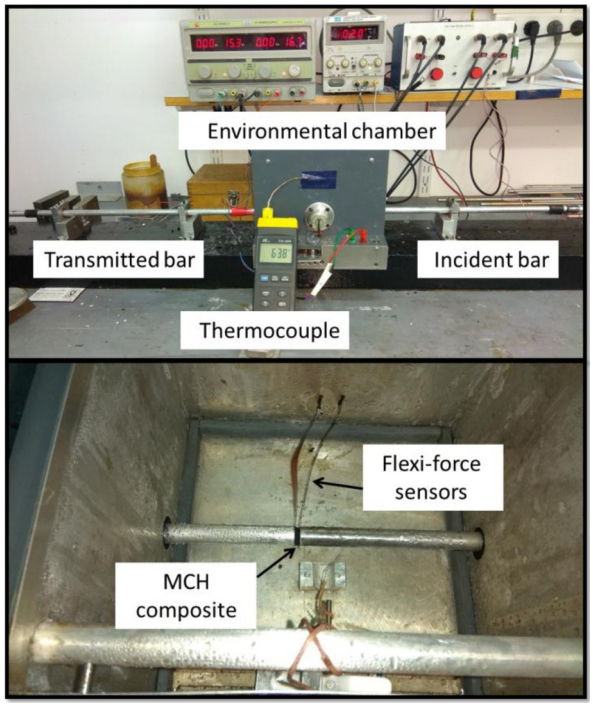

Fig. 1. Upper picture – modified Kolsky apparatus with the environmental chamber. Lower picture – MCH composite sample placed between the Kolsky's' bars with the Flexi-Force™ sensors.

2005; Kwon and Subhash, 2010; Benatar et al., 2003). While in conventional experiments the forces' amplitude ranges between 10^4 and 10^5N, in our experimental setup the measured forces were in the range of 1–20 N. These low force amplitudes significantly complicate the force measurement procedure and achievement of dynamic force equilibrium, which is essential for converting the conventional strain gauge signals into stress-strain curves (Davies and Hunter, 1963; Rotbaum and Rittel, 2014). In order to overcome this problem, a set of 201HT Flexi-force™ (FF) force sensors were cemented on the edges of the Hopkinson's bar, so that the interfacial forces were measured *directly* and not through signal analysis. A pulse shaper (Chen and Song, 2011; Frew et al., 2002), consisting of soft paper mixed with a carefully measured amount of molybdenum disulfide grease, was inserted between the striker and the incident bar. The pulse shaper is used to increase the rise time of the loading pulse and improves the specimens equilibrium due to reduced accelerations (Davies and Hunter, 1963). Additionally, to ensure conditions of constant 70 ± 3 °C and 100% relative humidity, a sealed heating chamber was employed.

In all the experiments, the area of the MCH specimens was in the range of 9–16 mm^2 and the specimen thickness was in the range of 2–4.5 mm. This geometry ensured that the sample diameter did not exceed that of the FF sensing area. These dimensions also minimize radial inertia effects which might affect the accuracy of the stress-strain determination (Song et al., 2007).

3. Results and discussion

3.1. Quasi-static compression

3.1.1. Particle material and size

The effect of different types of particles on the quasi-static mechanical response of the resulting composite MCHs was studied. Alumina, silica and boron carbide were used as the powder additives in various particle sizes and geometries. Silica and alumina are commonly used for modifying the properties and reinforcement of soft materials. Their advantage beside that of being inexpensive and available, is their active polyhydroxylated surfaces (Tsyganenko and Filimonov, 1973; Zhuravlev, 1987). Boron-carbide was chosen because of its interesting surface properties and potential in binding sugars, as well as its role in hardened ceramics (Domnich et al., 2011; Silver, 2007; Cafri et al., 2014).

Unless mentioned otherwise, the environmental temperature was set to 80 °C and the nominal strain rate is $0.5{\cdot}10^{-3}\ s^{-1}$. To correlate our results with previous results on pristine MCH, the composites had an MC polymer concentration of 56 g/L. A particle concentration of 3 g/L was used, due to preliminary finding that this was the optimal concentration for improvement of the mechanical properties of most of the MCH composites. Such a concentration is highly dilute (0.3% wt.), and therefore emphasizes the effect of the particles on the composite hydrogels. All composites presented in this work were verified to undergo thermogelation, thus ensuring that the inverse-freezing capability of the MCH was preserved.

Representative stress-strain curves of composite MCHs having different particle sizes and geometries are presented in Fig. 2.

Fig. 2 shows a significant enhancement of the flow-stress curves for a variety of particle-bearing composite MCHs. Of the studied MCH

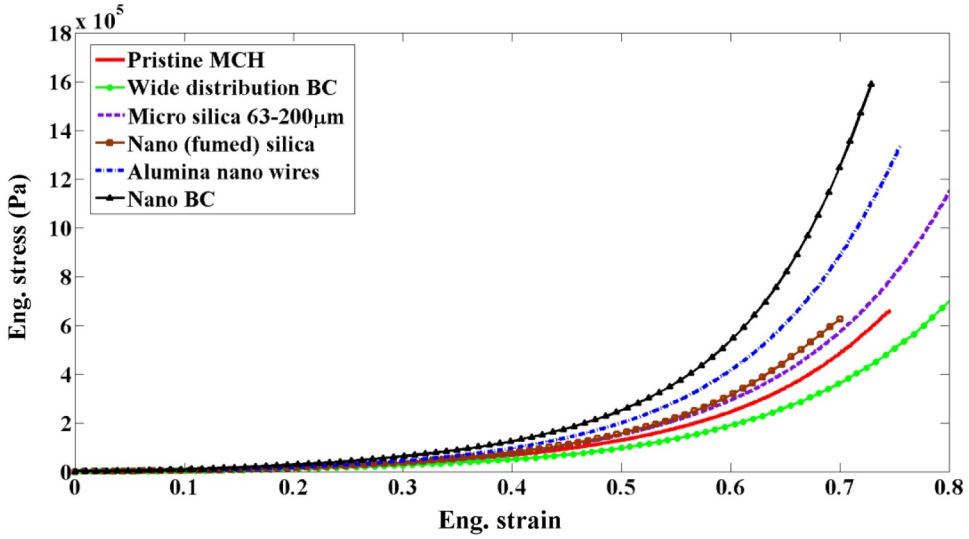

Fig. 2. Representative quasi-static flow curves of various MCH composites with particles differing in type, size and geometry. MC concentration: 56 gL^{-1}; particle concentration 3 $gL^{-1;}$ strain rate: 0.5·10–3 s^{-1}; temp: 80 ± 2 °C.

composites, only those with broad size distribution BC particles showed reduction in stress-flow compared to the pristine MCH. For the other composites, a ~10% - 270% increase of the flow-stress was found at 70% strain.

All the composites presented in Fig. 2, except the one with broad size distribution BC particles, have a slightly earlier transition from linear to non-linear hardening regime, implying that the particle reinforced gels harden at lower strains than the pristine MCHs (Rotbaum et al., 2017; Attard, 2003; Stammen et al., 2001; Djabourov, 1991).

Changes in the transition between the linear and the non-linear hardening regimes, as a function of the MC concentration, have been shown by McAllister et al. for pure MC hydrogels (McAllister et al., 2015). However, in the present study, the concentration of MC is kept constant (56 g L^{-1}), and these transitions are solely attributed to the presence of the particle additive.

At the micrometer scale, the reinforcement of the gel caused by the particles can be related to several factors: first, the small particles can be embedded between the MC chains network which causes significant local hardening leading to higher flow stress upon deformation. At much higher particle concentrations, long range particle clustering may be created, leading to load-bearing macro-sized structures. In our composite hydrogels, the particle concentration of 0.3% wt. is much smaller than the concentration needed to create such 3D rigid skeleton-like structures in the fishing net percolative models (Woignier et al., 2000; Stauffer and Aharony, 1994). Since the low concentration of particles in these composite MCHs renders long range inter-particle interaction highly unlikely, an alternative explanation could therefore stem from the interaction between particles and MC polymer structures within the gel.

Both silica and alumina particles are characterized by surface hydroxyl groups. These can either interact through hydrogen bonds with MC strands or even be replaced by oxygen atoms of the polymer, in both cases leading to polymers-particles supramolecular structures. In the case of boron carbide particles, the boron atom can coordinatively bind oxygen atoms of hydroxyl groups of MC either directly or indirectly via water molecules (Li et al., 2013). Such binding interactions, which are expected to be stronger than mere Van-Der Waals attractions between the polymer and the particle, could change the structure of the organic gel (Lott et al., 2013; Bodvik et al., 2010).

Fig. 2 shows that under the given experimental conditions, the difference in geometry and size of the micrometer-sized silica particles does not have much influence on the mechanical behavior of the composite MCHs. While both types of silica particles show slight improvement of flow stress compared to the pristine MCH, their flow-stress curves are very

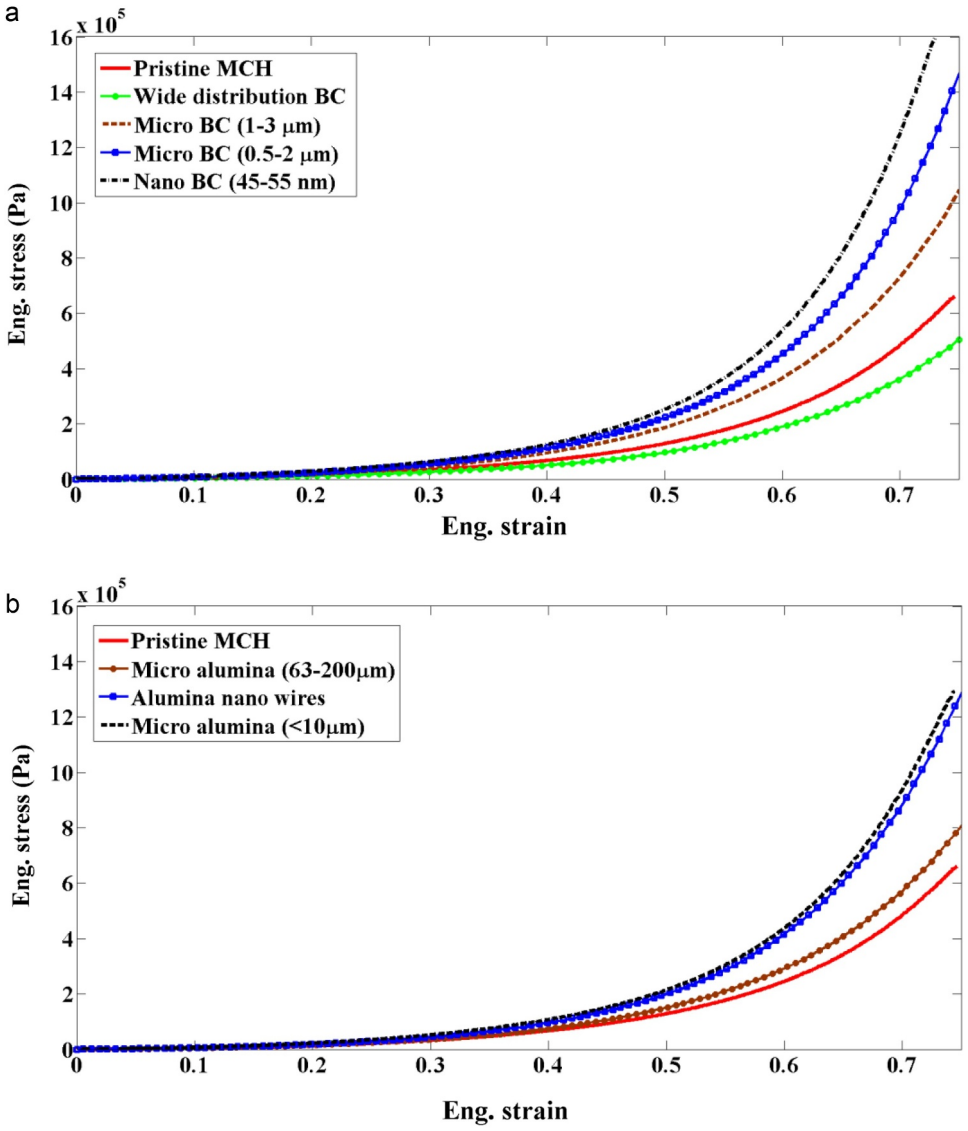

Fig. 3. Representative quasi-static flow curves of various MCH composites with particles of different sizes. MC concentration: 56 gL^{-1}; particle concentration 3 $gL^{-1;}$ strain rate: $0.5{\cdot}10^{-3}$ s^{-1}; temp: 80 ± 2 °C. (a) MCH composite with BC particles. (b) MCH composite with alumina particles.

similar despite one composite having the additive as a micrometer sized powder (purple curve), and the other having the additive with a multi-fold larger surface area and nanometric features (brown curve). Therefore, focus was directed to alumina and BC composites, and the exploration of the size-effect of these particles on their respective composites. Alumina/BC composites of MCH with different particle sizes were prepared and tested. Representative stress-strains curves are shown in Fig. 3a and b.

As shown in Figs. 3a and b, alumina-MCH and BC-MCH composites show a clear dependence of their mechanical response on the particle size. With the exception of wide-distribution BC, in both series, decrease of the particle size leads to increased flow-stress, with ratios of 270% and 194% at strains of 70% for BC-MCH and alumina-MC respectively, compared to the pristine hydrogel. For particles of the same type, the size effect can be explained by the particle surface-to-volume ratio consideration. As the particle size decreases, its ratio of surface area to total particle mass increases. Since all particles in this series were added at identical concentrations, smaller particles possess a larger surface area that is available for polymer binding, thereby causing the observed increase in the flow stress. Yet another possible reason for the increased performance of the smaller-sized particles is that they interact primarily with the smaller structural elements of the gel. The wide-distribution BC-MCH composite contains particles which are considerably larger than those of the other composites. These large particles may adsorb MC polymer strands in a manner that prevents these strands from participating in the load-bearing structures of the gel.

In contrast to boron carbides, particle additives of alumina display different effects on the composite. Micro-sized alumina in the larger scale (63–200 um) shows improved stress flow compared to the pristine MCH. Further decrease in particle size improves the stress flow even further, as both the smaller micrometer-sized alumina (<10um) and alumina nanowires composites show increase in stress flow. However, these two latter's stress curves are so similar to each other that we regard the differences between them to be negligible. Therefore, it can be concluded that from the size of lower micrometer range (<10 um), further decrease in particle size does not seem to contribute to stress flow increase of the composite. These results indicate that, for gel strengthening purposes, both particle material and size should be considered.

3.1.2. The effect of temperature

Pristine MCH undergoes further increase in stress-flow with temperature, even beyond its gelation temperature, indicating that the gelation process is not *complete* in gels that are at Tg (Rotbaum et al., 2017). In order to examine the effect of environmental temperature beyond that of the gelation point on the mechanical response of the composites, BC-MCH and alumina-MC composites containing the nano-sized particles at a concentration of 0.3% wt., were tested at temperatures between 65 °C and 100 °C, at a nominal strain rate of $0.5{\cdot}10^{-3}\ s^{-1}$ studied as a function of the temperature, Fig. 4a and b.

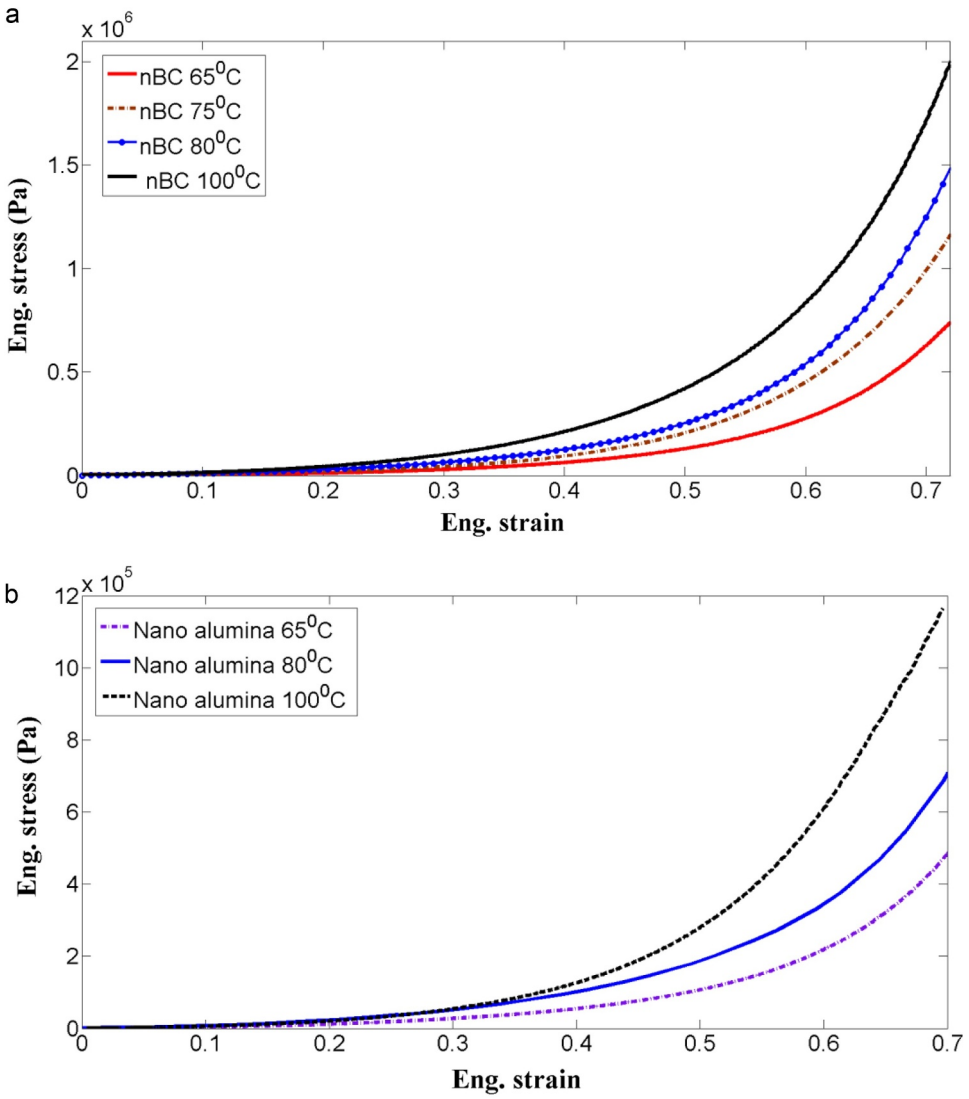

Fig. 4. Representative quasi-static flow curves of two MCH composites at various temperatures. MC concentration: 56 gL^{-1}; particle concentration 3 $gL^{-1;}$ strain rate: $0.5{\cdot}10^{-3}\ s^{-1}$ (a) MCH composite with nano-BC particles. (b) MCH composite with alumina nano-wires.

Fig. 4 clearly shows that for both composites, the particles enable considerable hardening of the gel with increasing temperature compared to pristine MCHs (Rotbaum et al., 2017). These findings on particle-mediated elevation of flow-stress with temperature imply that the particles help in harnessing MC polymer strands which are not part of the gel network to the load-bearing structures.

The strain rate sensitivity (SRS) investigation of the MCH composite with nano-particle additives was conducted in two stages. First, within the quasi-static loading regime ($5{\cdot}10^{-3}$–$2.5{\cdot}10^{-1}$ s^{-1}), then within the dynamic loading regime, using the split Hopkinson pressure bar.

Typical stress-strain curves of nBC and nano-alumina MCH composites at various strain rates are shown in Fig. 5a and b.

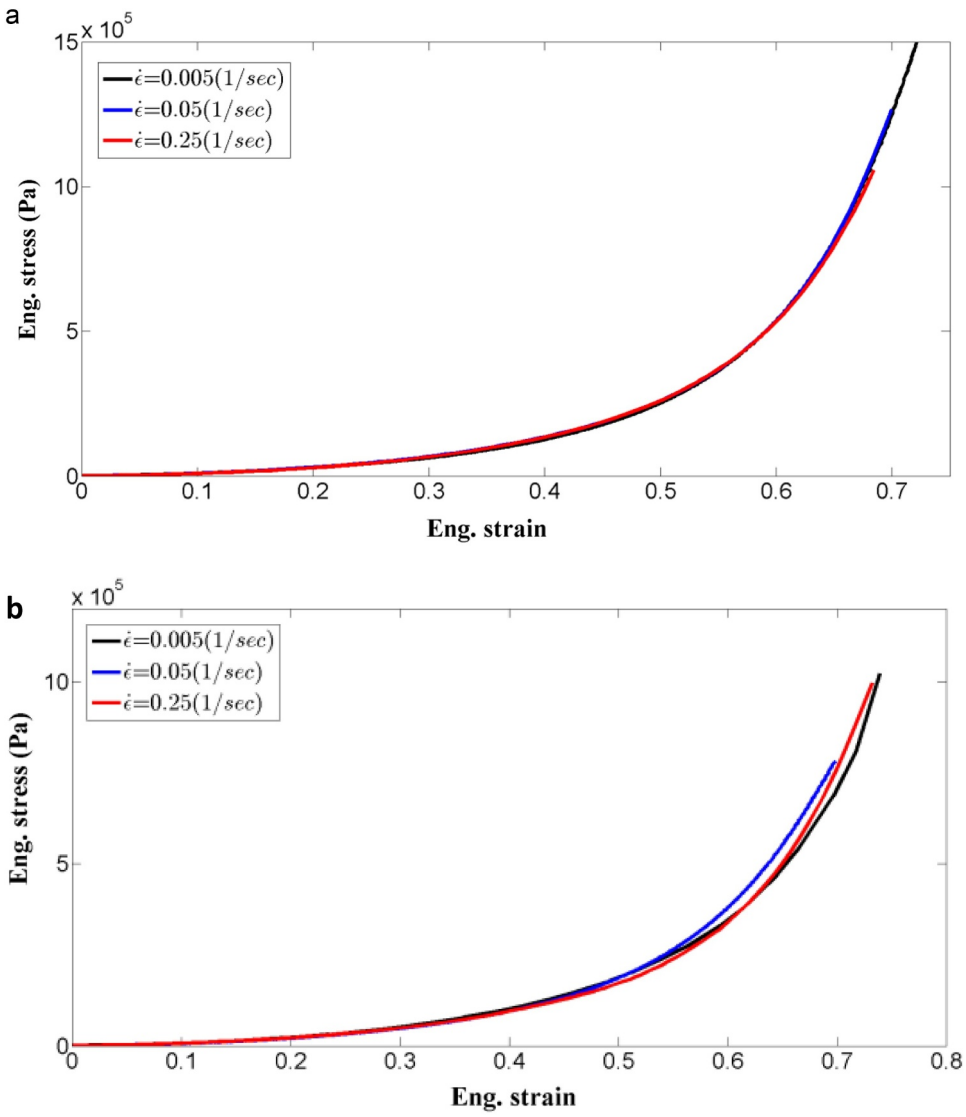

Fig. 5. Representative quasi-static flow curves of two MCH composites, at various strain rates. MC concentration: 56 gL^{-1}; particle concentration 3 $gL^{-1;}$ temp: 80 ± 2 °C. (a) MCH composite with nano-BC particles. (b) MCH composite with nano-alumina particles.

3.1.3. Strain-rate sensitivity

Several rheology experiments on aqueous solutions of MC solutions have shown that they behave as shear-thinning fluid (Li, 2002; Haque and Morris, 1993; Ethers, 1997; Floury et al., 2002), meaning that the mechanical resistance of the fluid to flow decreases with increasing shear-rates. However, it was recently reported that MC A7C gel exhibits a strong strain-rate sensitivity when submitted to dynamic loading. ($\sim 10^3$ s^{-1}) (Rotbaum et al., 2017). Such a contrasting observation can be explained by the vast difference in both strain and strain-rate values that characterize rheological tests on the one hand, and impact tests on the other hand (Parvari et al., 2018; McAllister et al., 2015).

According to Fig. 5a and Fig. 5b, there is no evidence for strain-rate sensitivity in the range of (quasi-static) strain-rates of the experiments, in accordance with earlier reported behavior of pristine MCH (Rotbaum et al., 2017).

3.2. Dynamic compression

Experiments at much higher strain-rates ~1000–2500 s^{-1}, were conducted using the split Hopkinson pressure bar (Kolsky apparatus) (Kolsky, 1949). Representative, true-stress true-strain curves of nBC-MCH are presented shown in Fig. 6.

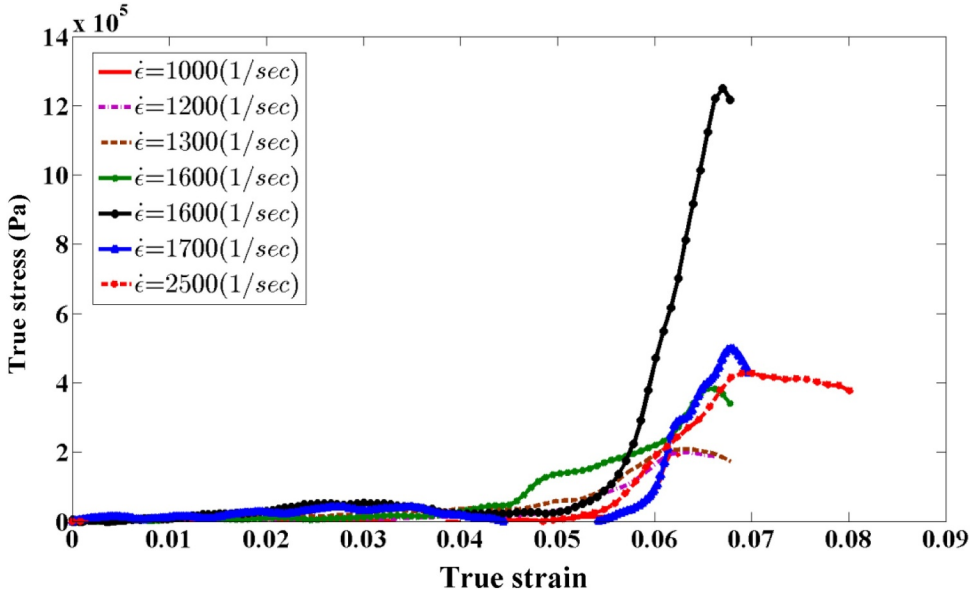

Fig. 6. Representative dynamic flow curves of two MCH-nBC composite at 70 °C at strain rate in the range of 1000–2500 $1/s^{-1}$. MC concentration: 56 gL^{-1}; particle concentration 3 $gL^{-1;}$ temp: 70 ± 2 °C.

Fig. 6 reveals a high degree of repeatability in the dynamic experiments. It also shows that once in the dynamic strain-rate regime, no apparent strain-rate sensitivity is observed. Almost negligible strain hardening develops up to a strain of approximately 0.05. From this value on, the composite hardens rapidly, leading to a failure at a relatively low strain ≤0.1, while no failure was observed in quasi-static loading even at large strains of the order of 0.9. Of note is the black curve in Fig. 6, representing a strain-rate of 1600 s^{-1}. While in most cases the specimen breaks into small fragments, interrupting the measurement at an overall low strain, in other cases when the specimen continues its compressive deformation, it adopts a thin gel sheet form and the failure strain increases. Such variations are commonly observed in Hopkinson bar experiments (Song and Chen, 2005).

In order to study the strain-rate sensitivity of MCH composite in a qualitative manner it is important to compare the dynamic flow-stress of different nanoparticle-MCH composite and pristine MCH to their respective static flow curves, Fig. 7. Since the stress flow of all the composites discussed in this report, is highly similar under quasi-static compression up to strains of about 0.2, the single quasi-static curve of the nBC-MCH composite is representative of all of them.

Even though no significant strain-rate sensitivity was observed within the ranges of 0.005–0.25 s^{-1} and 1000–2500 s^{-1},(Figs. 5 and 6), Fig. 7 shows clearly that the material response changes drastically when changing the loading conditions from static to dynamic. For example, for the nBC-MCH composite, at a strain of ~0.07 the strain-rate sensitivity is so strong that it leads to an increase of *more than 90 times* in the measured flow stress, 0.5 MPa and 54.6 KPa for the dynamic and the static curves respectively.

We surmise that this large increase of stresses in the dynamic regime in particle-MCH composites might be linked to the previously reported phenomenon of impact-induced gelation (Parvari et al., 2018). This gelation is induced by loading conditions that are similar to the dynamic regime in this present work, and occurs over time-scales that are relevant to those of the measurements shown in Fig. 7. As in the case of the gels increasing their flow- stress with increasing temperature beyond the gelation temperature discussed above, the presence of particles probably assists in harnessing additional polymers to join the load-bearing gel network and thus stiffen it upon dynamic loading.

It is well known that phase-transition is catalyzed by heterogeneities. For example, solid particles with appropriate surfaces provide

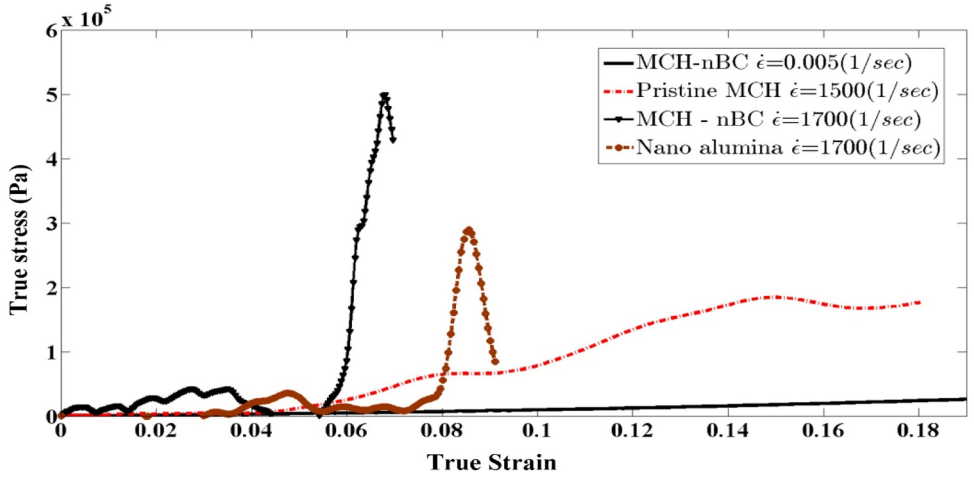

Fig. 7. A comparison between dynamic flow stress of pristine MCH and MCH nano-composite, to static response of different nBC -MCH composite.

nucleation sites for crystallization (Gránásy et al., 2007; Mer, 1952). The presence of solid particles within the MCH could serve as just such sites, at which gelation is more easily or rapidly achieved. Such facilitation of the phase-transition by particle-mediated nucleation would lead to enhanced mechanical performance especially in the dynamic loading regimes, where the fast response of the gel-forming solution is more critical than in the quasi-static, slower processes.

A possible support for this could be found in the relative low influence of the size of the alumina particles. Fig. 8 shows a comparison of the dynamic flow -stress of two composite MCHs containing alumina particles with different sizes and geometries.

originates from interaction between the surface of the particles and small structural elements of the MCH, such as polymer strands or fibrils. Another observation is that, compared to pristine MCH, MCH composites show larger increases in hardening with elevation of temperatures beyond the gelation point. This implies that the increased ability to recruit non-gelled polymers into the gel network is facilitated by the particles.

The strain-rate sensitivity study has shown that both in the quasi-static loading regime of $5{\cdot}10^{-3}$–$2.5{\cdot}10^{-1}$ s^{-1}, and in the dynamic loading regime of 1000–2000 s^{-1} there is no evidence for strain-rate sensitivity. With that, comparison of the two loading regimes, reveals a

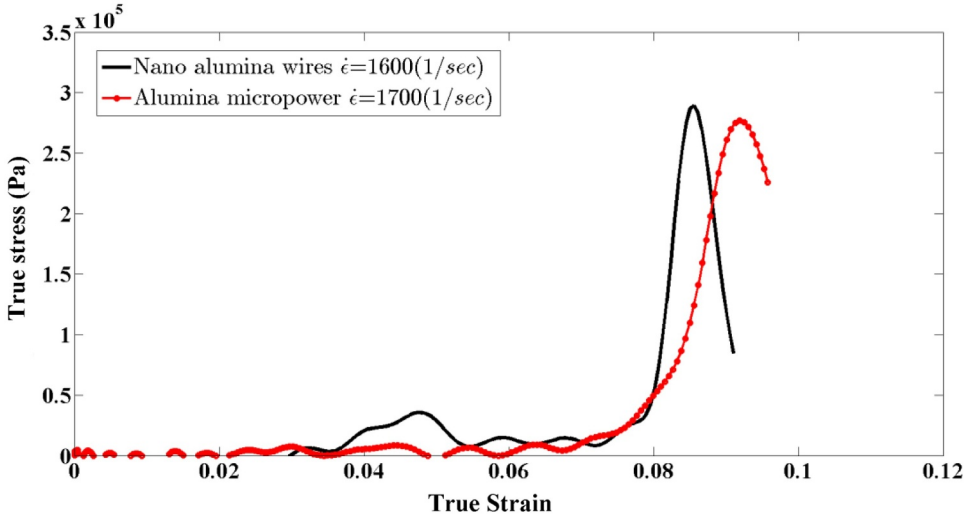

Fig. 8. A comparison between dynamic flow stress of MCH nano-alumina composite, at the similar size and different geometries. MC concentration: 56 gL^{-1}; particle concentration 3 $gL^{-1;}$ temp: 70 ± 2 °C.

Fig. 8 shows that the two dynamic curves are quite similar, and we regard the small difference in strain rate to be negligible and legitimate for comparison. This high similarity in the curves, despite their belonging to composites containing different particles, implies that the geometry and size difference of these particles does not play a significant role in the composites' dynamic response. This finding therefore supports the role of the particles to be that of local heterogeneous centers, in which the particles serve as nucleation sites, in which the differences between the particles are of lesser significance.

However, since the material composing the particle influences the response of MCH to dynamic loading, it is clear that surface species play a significant role in their interaction with the polymer strands.

4. Conclusions

This work reports on the improvement of the mechanical properties of MCH by transforming it into rigid particle-MCH composites. The unique ability of aqueous MC solutions to undergo heat-induced and shock-induced gelation into MCHs, makes this material worthy of further investigation. However, the mechanical properties of MCHs are currently insufficient for most engineering applications. We have thus presented an attempt to improve these properties by an approach to composite MCH with rigid particles. As part of this attempt, the particle types and sizes were studied for their effect on the resulting mechanical behavior of the composites.

Quasi-static compression experiments reveal that particles-MCH composites exhibit improved flow-stress, compared to pristine MCH, of up to 270% at 70% strain. Additionally, selection of the material and size of the particle allows tuning of the MCH flow-stress. The observation that for the same concentrations, the smaller particles will lead to better hardening may imply that the reinforcement primarily strong strain-rate sensitivity, as previously observed for pristine MCH. Both the alumina and nBC particles improve the composite's mechanical response to dynamic loadings. This is possibly due to the particles serving as "nucleation" sites for phase transition from liquid to gel upon the dynamic loading, which is similar in effect to the impact-type loading observed to cause gelation in pristine MC solutions. The nBC-MCH composite shows an extremely high ability to withstand dynamic-loaded stresses, compared to prisitne MCH.

Of all the investigated particles, the strongest reinforcing effect was observed for nanometric boron-carbide particles. This effect was shown for all strain-rates and temperatures considered in this study.

Although the detailed structure of MCH is not yet fully elucidated, the results herein could help shed light on some of their structural factors. The particles presented herein, which are at too small a concentration to form their own load-bearing super-structures, are presumed to interact directly with the polymers, in a manner that augments their ability to withstand both quasi-static and, more extensively, dynamic loading. These findings will also be used as primary data for a future constitutive material model.

Acknowledgment

This research was supported by the Technion Security Science and Technology Center, Grant 2024374.

Conflicts of interest

The authors declare no conflict of interests. G.P., Y. R. and D.R. are the inventors of a PCT application by the Technion, number PCT/IL2018/050606, "Inverse-freezing compositions and use thereof".

Supplementary materials

Supplementary material associated with this article can be found, in the online version, at doi:10.1016/j.mechmat.2019.02.013.

References

Arvidson, S., Lott, J., McAllister, J., Zhang, J., Bates, F., Lodge, T., Sammler, R., Li, Y., Brackhagen, M., 2012. Macromolecules 46, 300–309.
Attard, M.M., 2003. *Int. J. Solids Struct.* 40, 4353–4378.
Benatar, A., Rittel, D., Yarin, A., 2003. *J. Mech. Phys. Solids* 51, 1413–1431.
Bhimaraj, P., Burris, D.L., Action, J., Sawyer, W.G., Toney, C.G., Siegel, R.W., Schadler, L.S., 2005. Wear 258, 1437–1443.
Bodvik, R., Dedinaite, A., Karlson, L., Bergström, M., Bäverbäck, P., Pedersen, J.S., Edwards, K., Karlsson, G., Varga, I., Claesson, P.M., 2010. *Colloids Surf. A* 354, 162–171.
Borzacchiello, A., Ambrosio, L., 2009. Journal.
Cafri, M., Malka, A., Dilman, H., Dariel, M.P., Frage, N., 2014. *Int. J. Appl. Ceram. Technol.* 11, 273–279.
Chang, C., Zhang, L., 2011. *Carbohydr. Polym.* 84, 40–53.
Chen, W., Lu, F., Zhou, B., 2000. *Exp. Mech.* 40, 1–6.
Chen, W., Song, B., 2011. Split Hopkinson (Kolsky) Bar: Design, Testing and Applications. Springer.
Coleman, J.N., Khan, U., Blau, W.J., Gun'ko, Y.K., 2006. Carbon 44, 1624–1652.
Davies, E., Hunter, S., 1963. *J. Mech. Phys. Solids* 11, 155–179.
Djabourov, M., 1991. *Polym. Int.* 25, 135–143.
Domnich, V., Reynaud, S., Haber, R.A., Chhowalla, M., 2011. *J. Am. Ceram. Soc.* 94, 3605–3628.
Elias, L., Fenouillot, F., Majesté, J.-C., Cassagnau, P., 2007. Polymer 48, 6029–6040.
M.C. Ethers, *Midland, Michigan: Dow Chemical Company*, 1997.
Floury, J., Desrumaux, A., Axelos, M.A., Legrand, J., 2002. Food Hydrocolloids 16, 47–53.
Frew, D., Forrestal, M.J., Chen, W., 2002. *Exp. Mech.* 42, 93–106.
Gaharwar, A.K., Peppas, N.A., Khademhosseini, A., 2014. *Biotechnol. Bioeng.* 111, 441–453.
Gránásy, L., Pusztai, T., Saylor, D., Warren, J.A., 2007. *Phys. Rev. Lett.* 98, 035703.
Guo, Z., Pereira, T., Choi, O., Wang, Y., Hahn, H.T., 2006. *J. Mater. Chem.* 16, 2800–2808.
Haque, A., Morris, E.R., 1993. *Carbohydr. Polym.* 22, 161–173.
Haraguchi, K., 2007. *Curr. Opin. Solid State Mater. Sci.* 11, 47–54.
Hirrien, M., Chevillard, C., Desbrieres, J., Axelos, M., Rinaudo, M., 1998. Polymer 39, 6251–6259.
Hu, K., Shi, H., Zhu, J., Deng, D., Zhou, G., Zhang, W., Cao, Y., Liu, W., 2010. *Biomed. Microdevices* 12, 627–635.
Huang, W., Dalal, I.S., Larson, R.G., 2014. *J. Phys. Chem. B* 118, 13992–14008.
Kobayashi, K., Huang, C.-I., Lodge, T.P., 1999. Macromolecules 32, 7070–7077.
Kokabi, M., Sirousazar, M., Hassan, Z.M., 2007. *Eur. Polym. J.* 43, 773–781.
Kolsky, H., 1949. Journal 62, 676.
Kwon, J., Subhash, G., 2010. *J. Biomech.* 43, 420–425.
Li, L., 2002. Macromolecules 35, 5990–5998.
Li, X., Jiang, D., Zhang, J., Lin, Q., Chen, Z., Huang, Z., 2013. *J. Eur. Ceram. Soc.* 33, 1655–1663.
Lifshitz, J., Leber, H., 1994. *Int. J. Impact Eng.* 15, 723–733.
Lott, J.R., McAllister, J.W., Arvidson, S.A., Bates, F.S., Lodge, T.P., 2013. Biomacromolecules 14, 2484–2488.
McAllister, J.W., Lott, J.R., Schmidt, P.W., Sammler, R.L., Bates, F.S., Lodge, T.P., 2015. *ACS Macro Lett.* 4, 538–542.
Mer, V.K.L., 1952. *Ind. Eng. Chem.* 44, 1270–1277.
Miquelard-Garnier, G., Creton, C., Hourdet, D., 2008. Soft Matter 4, 1011–1023.
Nasatto, P.L., Pignon, F., Silveira, J.L., Duarte, M.E.R., Noseda, M.D., Rinaudo, M., 2015. Polymers 7, 777–803.
Parvari, G., Rotbaum, Y., Eichen, Y., Rittel, D, 2018. Impact-induced gelation in aqueous methylcellulose solutions. Chemical Communications 54 (89), 12578–12581.
Peppas, N.A., Ottenbrite, R.M., Park, K., Okano, T., 2010. Biomedical Applications of Hydrogels Handbook. Springer.
Plank, J., 2005. *Biopolym. Online* 10.
Richter, A., Paschew, G., Klatt, S., Lienig, J., Arndt, K.-F., Adler, H.-J.P., 2008. Sensors 8, 561–581.
Rotbaum, Y., Parvari, G., Eichen, Y., Rittel, D., 2017. Macromolecules.
Rotbaum, Y., Rittel, D., 2014. *Exp. Mech.* 54, 1–10.
Sarkar, N., 1979. *J. Appl. Polym. Sci.* 24, 1073–1087.
Schexnailder, P., Schmidt, G., 2009. *Colloid Polym. Sci.* 287, 1–11.
Schmidt, G., Malwitz, M.M., 2003. *Curr. Opin. Colloid Interface Sci.* 8, 103–108.
Schupper, N., Shnerb, N.M., 2005. *Phys. Rev. E* 72, 046107.
Serra, M., 2002. *Smart Mater. Bull.* 8, 7–8.
Shin, S.R., Jung, S.M., Zalabany, M., Kim, K., Zorlutuna, P., Kim, S.B., Nikkhah, M., Khabiry, M., Azize, M., Kong, J., 2013. ACS Nano 7, 2369–2380.
K.G. Silver, Georgia Institute of Technology, 2007.
Song, B., Chen, W., 2005. *Latin Am. J. Solids Struct.* 2, 113–152.
Song, B., Ge, Y., Chen, W., Weerasooriya, T., 2007. *Exp. Mech.* 47, 659.
Stammen, J.A., Williams, S., Ku, D.N., Guldberg, R.E., 2001. Biomaterials 22, 799–806.
Stauffer, D., Aharony, A., 1994. Introduction to Percolation Theory. CRC press.
Thoniyot, P., Tan, M.J., Karim, A.A., Young, D.J., Loh, X.J., 2015. *Adv. Sci.* 2.
Tsyganenko, A., Filimonov, V., 1973. *J. Mol. Struct.* 19, 579–589.
Wang, Y., Lapitsky, Y., Kang, C.E., Shoichet, M.S., 2009. *J. Controlled Rel.* 140, 218–223.
Woignier, T., Despetis, F., Alaoui, A., Etienne, P., Phalippou, J., 2000. *J. Sol-Gel Sci. Technol.* 19, 163–169.
Xie, F., Weiss, P., Chauvet, O., Le Bideau, J., Tassin, J.F., 2010. *J. Mater. Sci.* 21, 1163–1168.
Xu, Y., Li, L., Zheng, P., Lam, Y.C., Hu, X., 2004. Langmuir 20, 6134–6138.
Yahia, L., Chirani, N., Gritsch, L., Motta, F.L., 2015. *Biomed. Sci.*
Yan, D.X., Dai, K., Xiang, Z.D., Li, Z.M., Ji, X., Zhang, W.Q., 2011. *J. Appl. Polym. Sci.* 120, 3014–3019.
Zhang, Q., Archer, L.A., 2002. Langmuir 18, 10435–10442.
Zhang, X., Pint, C.L., Lee, M.H., Schubert, B.E., Jamshidi, A., Takei, K., Ko, H., Gillies, A., Bardhan, R., Urban, J.J., 2011. *Nano Lett.* 11, 3239–3244.
Zhuravlev, L., 1987. Langmuir 3, 316–318.